

Deep Signature FBSDE Algorithm

Qi Feng*

Man Luo[†]

Zhaoyu Zhang[‡]

Abstract

We propose a deep signature/log-signature FBSDE algorithm to solve forward-backward stochastic differential equations (FBSDEs) with state and path dependent features. By incorporating the deep signature/log-signature transformation into the recurrent neural network (RNN) model, our algorithm shortens the training time, improves the accuracy, and extends the time horizon comparing to methods in the existing literature. Moreover, our algorithms can be applied to a wide range of applications such as state and path dependent option pricing involving high-frequency data, model ambiguity, and stochastic games, which are linked to parabolic partial differential equations (PDEs), and path-dependent PDEs (PPDEs). Lastly, we also derive the convergence analysis of the deep signature/log-signature FBSDE algorithm.

1 Introduction

Motivation. Recent developments of numerical algorithm for solving high dimensional PDEs draw a great amount of attention in various scientific fields. In the seminal paper [38], deep learning technique was first introduced to study the numerical algorithms for high dimensional parabolic PDEs. The deep learning BSDE method is based on the non-linear Feynman-Kac formula, which provides the equivalent relations between parabolic PDEs and Markovian backward stochastic differential equations (BSDEs) (see e.g. [30]). When the system does not have Markovian property, e.g. path-dependent property involved, the BSDE is equivalent to a path-dependent PDE (PPDE), which was first introduced in

*Department of Mathematics, University of Michigan, Ann Arbor, MI 48109-1043. Email: qif@umich.edu

[†]Department of Mathematics, University of Southern California, Los Angeles, CA 90089-2532. Email: manl@usc.edu

[‡]Department of Mathematics, University of Southern California, Los Angeles, CA 90089-2532. Email: zzhang51@usc.edu

[11] for path-dependent option pricing problem. The deep learning BSDE method has been recently extended to design numerical algorithms for PPDEs. The path-dependent property introduces extra complexity in the numerical scheme, and it returns a high dimensional problem even if the original space variable is low dimensional. In this study, we shall focus on the numerical solutions for the corresponding Markovian and non-Markovian FBSDEs.

For the deep learning BSDE method [38], it shows the efficiency of machine learning in solving high dimensional parabolic PDEs but subject to small Lipschitz constants or equivalently small time duration. The exponential stopping time strategy has been introduced in [35] to extend the time duration. However, both algorithms are still using the deep neural network combined with standard Euler scheme in essence, which makes it sensitive to the time discretization. Namely, the time dimension is still large for long time duration, which may take a long time to train the deep neural network (DNN) model. Furthermore, the deep learning BSDE method is not robust to missing data. If we miss a proportion of our data (e.g. data points in the Euler scheme), the accuracy will be affected. In particular, this is the same type of difficulty when dealing with high frequency data. In this case, one has to down-sample the stream data to a coarser time grid to feed it into the DNN-type algorithm. It may miss the microscopic characteristic of the streamed data and render lower accuracy. On the other hand, the high frequency and path-dependent features show up naturally in option pricing problems and non-linear expectations within various financial contexts, e.g. limit order book [5, 6, 9, 17, 24, 26], nonlinear pricing [30, 39], Asian option pricing [29], model ambiguity [3, 4, 10, 16], stochastic games and mean field games [13, 33], etc.

Our work. Motivated by these problems, we introduce the deep signature transformation into the recurrent neural network (RNN) model to solve BSDEs. The “signature” is defined as an iterated integral of a continuous path with bounded p -variation, for $p > 1$, which is a recurring theme in the rough path theory introduced by T. Lyons [25]. The “signature” has recently been used to define kernels [8, 21, 28] for sequentially ordered data in the corresponding reproducing kernel Hilbert space (RKHS). This idea is further developed in [20] to design “deep signature” by combining the kernel method and DNN. Furthermore, the “deep signature” has been used in RNN to study controlled differential equations in [23]. The signature approach also provides a non-parametric way for extraction of characteristic features from the data, see e.g. [22]. The data are converted into a multi-dimensional path through various embedding algorithms and then processed for computation of individual

terms of the signature, which captures certain information contained in the data. The advantage of this signature method is that this method can deal with high frequency data, and is not sensitive to the time discretization. Motivated by this idea, we propose to combine the signature/log-signature transformation and RNN model to solve the FBSDEs, which should have a much coarser time partition, a better downsampling effect, and more robust to the high-frequency data assumptions.

Related works. The numerical algorithm for solving PPDE with path dependent terminal condition (first type PPDE) has been recently studied in [36, 37] by using recurrent neural network. The second type PPDE arises from the Volterra SDE setting, where the non-Markovian property is introduced by the forward process instead of the terminal condition. The numerical algorithms for the option pricing problem in the Volterra SDEs setting has been recently studied in [19, 35] by using deep learning, [2] by using regularity structures, and [12] by using cubature formula.

However, none of these works consider the high frequency data features in the algorithm. Neither do they consider the longer time duration in the model. Furthermore, we also provide the convergence analysis of our algorithm after introducing the signature/log-signature transformation layer into the RNN model.

2 Algorithms

2.1 Signature and signature transformation

In this section, we introduce the preliminary facts about the signature from the rough path theory [25] and the signature transformation [23] we used in the algorithm. In general, for a bounded variation path $x_t \in \mathbb{R}^d$, for $t \in [0, T]$, the signature of x (up to order N) is defined as the iterated integrals of x . More precisely, for a word $J = (j_1, \dots, j_k) \in \{1, \dots, d\}^k$ with size $|J| = k$,

$$\begin{aligned} \text{Sig}_N(x)_t &= \sum_{k=0}^N \int_{0 < t_1 < \dots < t_k < t} dx_{t_1} \otimes \dots \otimes dx_{t_k}, \quad t \in [0, T], \\ &= \left(1, \sum_{j=1}^d \int_0^t dx_{t_1}^j, \dots, \sum_{|J|=N} \int_{0 < t_1 < \dots < t_N < t} dx_{t_1}^{j_1} \dots dx_{t_N}^{j_N} \right) \end{aligned} \quad (2.1)$$

where we use the convention that $\text{Sig}_0(x)_t \equiv 1$. The signature $\text{Sig}_N(x)_t$ lives in a strict subspace $\mathbb{G}_N(\mathbb{R}^d) \subset T_N(\mathbb{R}^d)$, known as the free Carnot group over \mathbb{R}^d of step N , where $T_N(\mathbb{R}^d) = \bigoplus_{k=0}^N (\mathbb{R}^d)^{\otimes k}$ is the truncated tensor algebra over \mathbb{R}^d . Furthermore, the exponential map defines the diffeomorphism from the Lie algebra $\mathfrak{g}_N(\mathbb{R}^d)$ to the Lie group $\mathbb{G}_N(\mathbb{R}^d)$, namely

$$\mathbb{G}_N(\mathbb{R}^d) = \exp(\mathfrak{g}_N(\mathbb{R}^d)), \quad (2.2)$$

where $\mathfrak{g}_N(\mathbb{R}^d)$ is the Lie sub-algebra of $T_N(\mathbb{R}^d)$ generated by the canonical basis $e_i, i = 1, \dots, d$, of \mathbb{R}^d , and the Lie bracket is given by $[a, b] = a \otimes b - b \otimes a$. Thus, the log signature lives in the linear space $\mathfrak{g}_N(\mathbb{R}^d)$, and we denote logarithm of the signature of the path x as $\text{LS}(x)$. Let $\pi_m(\cdot)$ be the projection map of the signature and the log signature at order m . We denote $\text{LS}_m(X) = \pi_m(\text{LS}(x))$ as the truncated log signature of a path x of order m . We introduce the following standard treatment when computing the signature of a path together with the time parameter.

Definition 2.1. *Given a path $x : [a, b] \rightarrow \mathbb{R}^d$, we define the corresponding time-augmented path by $\hat{x}_t = (t, x_t)$, which is a path in \mathbb{R}^{d+1} .*

We should remark here that a bounded p -variation path is essentially determined by its truncated signature at order $\lfloor p \rfloor$ (e.g. [14][Chapter 7]). This means that essentially no information is lost when applying the signature transform of a path at certain order without using the whole signature process.

Proposition 2.2 (Universal nonlinearity, [1], see also [20] Proposition A.6). *Let F be a real-valued continuous function on continuous piecewise smooth paths in \mathbb{R}^d and let \mathcal{K} be a compact set of such paths. Then for all $x \in \mathcal{K}$ and $\forall \varepsilon$, there exists a linear functional \mathcal{L} such that,*

$$|F(x) - \mathcal{L}(\text{Sig}(x))| \leq \varepsilon. \quad (2.3)$$

We introduce the signature and the log signature layer in [23].

Definition 2.3 (Signature and log Signature Sequence Layer). *Consider a discrete d -dimensional time series $(x_{t_i})_{i=1}^n$ over time interval $[0, T]$. A (log) signature layer of degree m is a mapping from $\mathbb{R}^{d \times n}$ to $\mathbb{R}^{\hat{d} \times N}$, which computes $(\text{Sig}_k)_{k=0}^{N-1}$ (or $(\text{LS}_k)_{k=0}^{N-1}$) as an output for any x , where Sig_k (or LS_k) is the truncated (log) signature of x over time interval*

$[u_k, u_{k+1}]$ of degree m as follows:

$$\text{Sig}_k = \pi_m(\text{Sig}_{[u_k, u_{k+1}]}) \text{, (or } \text{LS}_k = \pi_m(\text{LS}_{[u_k, u_{k+1}]}) \text{)}, \quad (2.4)$$

where $k \in \{0, 1, \dots, N-1\}$ and \hat{d} is the dimension of the truncated (log) signature.

2.2 Main algorithms

In this section, We consider the following Markovian FBSDE,

$$\text{(M)} \begin{cases} X_t &= x + \int_0^t b(s, X_s) ds + \int_0^t \sigma(s, X_s) dW_s, \\ Y_t &= g(X_T) + \int_t^T f(s, X_s, Y_s, Z_s) ds - \int_t^T Z_s dW_s, \end{cases} \quad (2.5)$$

and the non-Markovian FBSDE,

$$\text{(NM)} \begin{cases} X_t &= x + \int_0^t b(s, X_s) ds + \int_0^t \sigma(s, X_s) dW_s, \\ Y_t &= g(X_{\cdot \wedge T}) + \int_t^T f(s, X_{\cdot \wedge s}, Y_s, Z_s) ds - \int_t^T Z_s dW_s, \end{cases} \quad (2.6)$$

for $t \in [0, T]$. In both the Markovian (M) and non-Markovian (NM) FBSDEs system above, we denote $\{W_s\}_{0 \leq s \leq T}$ as \mathbb{R}^d -valued Brownian motion. Throughout the paper, unless otherwise stated, the process X, Y , and Z take values in $\mathbb{R}^{d_1}, \mathbb{R}^{d_2}$, and $\mathbb{R}^{d_2 \times d}$, respectively. We denote $g(X_T)$ as the state dependent terminal condition and denote $g(X_{\cdot \wedge T})$ as the terminal condition depending on the path of X , which corresponds to the the payoff function in the option pricing problem. The pair $(Y_t, Z_t)_{0 \leq t \leq T}$ solves the BSDE in (M) and (NM) respectively.

We present signature/ log-signature FBSDE numerical schemes in detail. We first partition the time horizon $[0, T]$ into n time steps with a mesh size $\Delta t := T/n$, and the time partition is given by $0 = t_0 < t_1 < \dots < t_n = T$. The state process X is generated from Euler scheme as

$$X_{t_{i+1}}^n = X_{t_i}^n + b(t_i, X_{t_i}^n) \Delta t + \sigma(t_i, X_{t_i}^n) \Delta W_{t_{i+1}}, \quad (2.7)$$

where $\Delta W_{t_{i+1}} := W_{t_{i+1}} - W_{t_i}$ denotes the increment of the Brownian motion. Next, for some $k \in \{a \in \mathbb{Z}^+ : n/a \in \mathbb{Z}^+\}$, we partition the time interval $[0, T]$ into $\tilde{n} := n/k$ segmentations with step size $\Delta u := k \Delta t$. The segmentation can be written as $0 = u_0 < u_1 (= t_k) < \dots < u_{\tilde{n}} = T$. Then we compute the signature/log-signature¹ of the forward

¹The numerical implementation of the signature/log-signature transformation was borrowed from [34].

process X truncated at order m based on the segmentation $(u_i)_{1 \leq i \leq \tilde{n}}$, which is denoted as $(\pi_m(\text{Sig}(X^n)_1), \dots, \pi_m(\text{Sig}(X^n)_{\tilde{n}}))$. Moreover, we approximate the process Z using a recurrent neural network (RNN) with truncated signature / log-signature at order m as the inputs. Namely, we denote

$$Z_{u_i}^{\theta, \text{Sig}} := \mathcal{R}^\theta(\pi_m(\text{Sig}(X^n)_0), \dots, \pi_m(\text{Sig}(X^n)_{i-1})), \quad (2.8)$$

for $i \in \{1, \dots, \tilde{n}\}$, which is the output of the RNN² with truncated signature of forward process X at order m as the inputs. Similarly, we denote

$$Z_{u_i}^{\theta, \text{LS}} := \mathcal{R}^\theta(\pi_m(\text{LS}(X^n)_0), \dots, \pi_m(\text{LS}(X^n)_{i-1})) \quad (2.9)$$

as the output of RNN with log signature inputs. Then, the discrete scheme of Y for the Markovian BSDE is given as below,

$$Y_{u_i}^{\tilde{n}, \text{Sig}} := Y_{u_{i-1}}^{\tilde{n}, \text{Sig}} - f(u_{i-1}, X_{u_{i-1}}^n, Y_{u_{i-1}}^{\tilde{n}, \text{Sig}}, Z_{u_{i-1}}^{\theta, \text{Sig}}) \Delta u_i + Z_{u_{i-1}}^{\theta, \text{Sig}} \Delta W_{u_i}, \quad \text{for (M)}. \quad (2.10)$$

Similarly, for the non-Markovian problem, we define

$$\bar{Y}_{u_i}^{\tilde{n}, \text{Sig}} := \bar{Y}_{u_{i-1}}^{\tilde{n}, \text{Sig}} - f(u_{i-1}, X_{[0, u_{i-1}]}^n, \bar{Y}_{u_{i-1}}^{\tilde{n}, \text{Sig}}, Z_{u_{i-1}}^{\theta, \text{Sig}}) \Delta u_i + \bar{Z}_{u_{i-1}}^{\theta, \text{Sig}} \Delta W_{u_i}, \quad \text{for (NM)}, \quad (2.11)$$

where $\Delta W_{u_{i+1}} := W_{u_{i+1}} - W_{u_i}$. Lastly, the objective is to minimize the loss function $l(\theta, Y_0, Z_0) := \mathbb{E}[(Y_T^{\tilde{n}, \text{Sig}} - g(X_T^n))^2]$ (or $l(\theta, Y_0, Z_0) := \mathbb{E}[(Y_T^{\tilde{n}, \text{Sig}} - g(X_{\wedge T}^n))^2]$ for non-Markovian FBSDE), and update parameters θ by stochastic gradient descent. The algorithms for log-signature follows similarly by changing the Sig layer with LS layer in the algorithm. The full algorithm for the Sig-layer FBSDE (or LS-layer FBSDE) is presented in Algorithm 1.

We keep the following standard assumptions on the coefficients for FBSDEs.

Assumption 1. *Let the following assumptions be in force.*

- b, σ, f, g are deterministic taking values in \mathbb{R}^{d_1} , $\mathbb{R}^{d_1 \times d}$, \mathbb{R}^{d_2} , \mathbb{R}^{d_2} , respectively; and $b(\cdot, 0), \sigma(\cdot, 0), f(\cdot, 0, 0, 0)$ and $g(0)$ are bounded.
- b, σ, f, g are C^k -smooth with respect to all variables (t, x, y, z) for any desired $k \in \mathbb{N}_+$ and all derivatives are bounded by constant L .

²In particular, the recurrent network in this paper is the LSTM network [18].

Algorithm 1 Deep signature/log-signature FBSDE algorithm.

- 1: Initialize Y_0, Z_0 . Initialize mesh size Δt , mini-batch size M , total number of paths \hat{N} , signature order m , number of segments \tilde{n} , loss threshold ε .
 - 2: Generate data. (1) Simulate \hat{N} paths of Brownian motions $(W_{t_1}^j, \dots, W_{t_n}^j)_{1 \leq j \leq \hat{N}}$ and (2) generate \hat{N} paths of state processes $(X_{t_1}^{j,n}, \dots, X_{t_n}^{j,n})_{1 \leq j \leq \hat{N}}$. (3) Compute signatures of state processes $(\pi_m(\text{Sig}(X^{j,n})_0), \dots, \pi_m(\text{Sig}(X^{j,n})_{\tilde{n}-1}))_{1 \leq j \leq \hat{N}}$ (or $(\pi_m(\text{LS}(X^{j,n})_0), \dots, \pi_m(\text{LS}(X^{j,n})_{\tilde{n}-1}))_{1 \leq j \leq \hat{N}}$).
 - 3: **while** $\text{loss}(\theta, Y_0, Z_0) > \varepsilon$ **do**
 - 4: Randomly select a mini-batch of data, with batch size M .
 - 5: **for** $i \in \{1, \dots, \tilde{n}\}$
 - 6: $Z_{u_i}^{j,\theta,\text{Sig}} = \mathcal{R}^\theta(\pi_m(\text{Sig}(X^{j,n})_0), \dots, \pi_m(\text{Sig}(X^{j,n})_{i-1}))$.
 - 7: (or $Z_{u_i}^{j,\theta,\text{LS}} = \mathcal{R}^\theta(\pi_m(\text{LS}(X^{j,n})_0), \dots, \pi_m(\text{LS}(X^{j,n})_{i-1}))$).
 - 8: Compute $Y_{u_{i+1}}^{j,\tilde{n},\text{Sig}}$ from Euler scheme (2.10).
 - 9: **end**
 - 10: Compute $\text{loss}(\theta, Y_0, Z_0) = \frac{1}{M} \sum_{j=1}^M (Y_T^{j,\tilde{n},\text{Sig}} - g(X_T^{j,n}))^2$ for problem (M).
 $\text{loss}(\theta, Y_0, Z_0) = \frac{1}{M} \sum_{j=1}^M (Y_T^{j,\tilde{n},\text{Sig}} - g(X_{\cdot \wedge T}^{j,n}))^2$ for problem (NM).
 - 11: (or Compute $\text{loss}(\theta, Y_0, Z_0) = \frac{1}{M} \sum_{j=1}^M (Y_T^{j,\tilde{n},\text{LS}} - g(X_T^{j,n}))^2$ for problem (M).
 $\text{loss}(\theta, Y_0, Z_0) = \frac{1}{M} \sum_{j=1}^M (Y_T^{j,\tilde{n},\text{LS}} - g(X_{\cdot \wedge T}^{j,n}))^2$ for problem (NM).)
 - 12: Minimize loss, and update θ by stochastic gradient descent.
-

We are now ready to present the universality approximation property of deep signature/log-signature Markovian FBSDE.

Lemma 2.4. *Let **Assumption 1** be in force. Assume that $kh < \delta$ for any small $\delta > 0$, for any given $T > 0$, for some constant $C > 0$ depending on T and L in **Assumption 1**, and for any $\varepsilon > 0$, there exists recurrent neural network \mathcal{R}^θ , such that*

$$\sum_{i=0}^{\tilde{n}-1} \mathbb{E} \left[\int_{u_i}^{u_{i+1}} |Z_t - Z_{u_i}^{\theta, \text{Sig}}|^2 dt \right] \leq C[1 + |x|^2]\delta + \varepsilon.$$

Furthermore, we have the following estimate.

Theorem 2.5. *Let **Assumption 1** be in force. Assume that $kh < \delta$ for any small $\delta > 0$, for any given $T > 0$, for some constant $C > 0$ depending on T and L in **Assumption 1**, and for any $\varepsilon > 0$, there exists recurrent neural network \mathcal{R}^θ , such that*

$$\max_{0 \leq i \leq \tilde{n}} \mathbb{E} \left[\sup_{u_i \leq t \leq u_{i+1}} |Y_t - Y_{u_i}^{\tilde{n}, \text{Sig}}|^2 \right] \leq C[1 + |x|^2 + \varepsilon]\delta.$$

The same estimates follow after replacing $Z_{\cdot}^{\theta, \text{Sig}}$ with $Z_{\cdot}^{\theta, \text{LS}}$ in Lemma 2.4 and Theorem 2.5. We proved Lemma 2.4 and Theorem 2.5 in Section 4.1. Similar results hold true for non-Markovian FBSDE as well, we postpone the analysis in Section 4.2

3 Numerical results

In this section, we implement our algorithm to a wide range of applications including European call option, lookback option under Black-Scholes model, European call option under Heston model, and a high dimensional example etc.³. In summary, our Sig/LS-FBSDE method has the following advantages over other numerical methods in the current literature:

1. Our algorithm is capable to find a more accurate solution to the FBSDE.
2. Our algorithm is capable to approximate the true solution efficiently in terms of computation time.

³The code could be found in the following URL link: <https://github.com/zhaoyu-zhang/Sig-logSig-FBSDE>. The desktop we used in this study is equipped with an i7-8700 CPU and a RTX 2080Ti GPU. For all the examples in this paper, we generated in total of $\hat{N} = 100,000$ paths for the forward processes. 1,000 paths were used to test, and the rest were used to train the neural network.

3. Our algorithm is capable to handle high frequency data in a long time duration. The results are accurate and computation times are efficient.
4. Our algorithm is capable to handle high dimensional and non-linear scenarios.

Throughout this section, we denote $(\Omega, \mathcal{F}, (\mathcal{F}_t)_{t \geq 0}, \mathbb{P})$ as the filtered probability space and denote \mathbb{Q} as the risk neutral measure.

3.1 Best Ask Price for GBM European Call Option

The limit order book spread has been extensively investigated through *No Arbitrage Bound/No Good Deal bound* in incomplete markets [6, 7, 9, 17, 26, 27]. Traditionally, under a risk neutral measure \mathbb{Q} , one may assume the underlying asset X follows a geometric Brownian motion i.e.,

$$dX_t = X_t(r_t dt + \sigma_t dW_t), \quad X_0 = x_0,$$

where W_t is a standard Brownian motion under \mathbb{Q} . For implementation convenience, we usually use constant r and σ to represent r_t and σ_t in numerical examples. By no good deal theory, the best ask price for the European call option at level κ (κ can be thought as the bound for girsanov kernels) can be represented as

$$P^{ask, \kappa} = \sup_{\mathbb{P} \in \mathcal{Q}^{ngd, \kappa}} \mathbb{E}^{\mathbb{P}}[\beta_0^T (X_T - K)^+], \quad (3.12)$$

where the set $\mathcal{Q}^{ngd, \kappa}$ is nonempty and called the no good deal pricing set at level κ , β_t^T is the discount factor defined by fixed risk-free interest rate r_t . More details can be referred to [5, 7, 24, 26]. In our setting, we define $\mathcal{Q}^{ngd, \kappa}$ as follow

$$\mathcal{Q}^{ngd, \kappa} := \left\{ \mathbb{Q}^\theta : \frac{d\mathbb{Q}^\theta}{d\mathbb{Q}} = M_T(\lambda^\theta, W); \sup_{t \in [0, T]} \|\lambda_t^\theta\| \leq \kappa \right\}, \quad (3.13)$$

where $M_T(\lambda^\theta, W) := \exp\{\int_0^T \lambda_t^\theta dW_t - \frac{1}{2} \int_0^T \|\lambda_t^\theta\|^2 dt\}$, the process λ_t^θ denote all possible girsanov kernels and their bound is κ .

Remark 1. *There are several notions to introduce the kernel function λ_t^θ . The kernel ambiguity introduced by drift uncertainty with discount factor $\beta_0^T(r^\theta)$ has been recently studied in [24]. Here we work in a simplified version, where we consider the discount factor fixed, we define $\lambda_t^\theta := \sigma_t^{-1}(\alpha_t^\theta - r_t \mathbf{1})$, where $\alpha_t^\theta \in \Lambda$, and $\Lambda = \{x \in \mathbb{R}^d, (x - r_t \mathbf{1})^\top \sigma_t \sigma_t^\top (x - r_t \mathbf{1}) \leq$*

$\kappa^2, \forall t \in [0, T]\}$. The main motivation to consider a fixed interest rate r_t instead of r_t^θ is that we could numerically compute the lower and upper bound by using the empirical calibration of r_t from the market data.

With the specification of the pricing measure set $\mathcal{Q}^{ngd, \kappa}$ in (3.13), we can show that (3.12) is closely linked to the following BSDE. The proof follows from the comparison theorem for BSDEs, and we refer details in [31].

Theorem 3.1. *Assume no good deal assumption, then one can obtain that the best ask/bid price (3.12) at level κ are unique solutions to the following BSDEs when $t = 0$*

$$Y_t^\pm = \xi_T + \int_t^T G^\pm(X_t, Y_t, Z_t) dt - \int_t^T Z_t dW_t, \quad (3.14)$$

where $\xi_T := (X_T - K)^+$ and G^\pm are optimised drivers over all possible kernels in (3.13),

$$G^-(x, y, z) = \min_{\|\lambda^\theta\| \leq \kappa} f(x, y, z, \lambda^\theta) \quad \text{and} \quad G^+(x, y, z) = \max_{\|\lambda^\theta\| \leq \kappa} f(x, y, z, \lambda^\theta).$$

Here we define $f(x, y, z, \lambda^\theta) := -ry + z\lambda^\theta$. Furthermore, we can obtain the optimised drivers as follow

$$G^\pm(x, y, z) = \pm\kappa\|z\| - ry.$$

In this example, we implement 1-dimensional best ask scenario for (3.14), and we compare results from our signature methods with simple neural network method. We choose the following parameters for the simulation $x_0 = 100, \sigma = 0.20, r = 0.05, \kappa = 0.05, K = 80, T = 1, m = 3, \tilde{n} = 5$, and batch size 1000.

Table 1: Best ask price for GBM European call option

Simple NN	Sig-LSTM	Sig-LSTM	Sig-LSTM	Sig-LSTM
$n = 100$	$\tilde{n} = 5, n = 100$	$\tilde{n} = 5, n = 500$	$\tilde{n} = 5, n = 1000$	$\tilde{n} = 5, n = 5000$
25.526	25.48	25.46	25.46	25.45

As we see from Table 1, our algorithm combining signature with LSTM neural network (labeled as Sig-LSTM) outperforms the simple neural network method in terms of efficiency, our algorithm runs 20 times faster than simple neural network approach with $n = 100$. This is what we should expect, since for each iteration our algorithm runs 5 steps segmented by

signature ($\tilde{n} = 5$) instead of 100 steps ($n = 100$) in the simple neural network approach with Euler scheme. Also, as we can see in Table 1, the result converges to 25.45 when n increases. More accuracy and time efficiency results comparisons are illustrated in the lookback option example, which is a path dependent option.

3.2 Lookback Option Example

In this example, we consider the classical Black-Scholes model setting. Under the risk neutral measure \mathbb{Q} , the stock prices $(X_t)_{t \geq 0}$ follows a geometric Brownian Motion with constant interest rate r , and volatility σ ,

$$dX_t = rX_t dt + \sigma X_t dW_t, \quad X_0 = x_0.$$

Lookback option is one of the path-dependent financial derivatives. A lookback call option with floating strike is given by the payoff function

$$g(X_{[0,T]}) = X_T - \inf_{0 \leq t \leq T} X_t.$$

It is clear that the option price Y_t has the form

$$Y_t = e^{-r(T-t)} \mathbb{E}^{\mathbb{Q}}[g(X_{[0,T]}) | \mathcal{F}_t].$$

Fortunately, Y_t has an explicit solution, (e.g. [29]),

$$Y_t = X_t \Phi(a_1) - m_t e^{-r(T-t)} \Phi(a_2) - X_t \frac{\sigma^2}{2r} \left(\Phi(-a_1) - e^{-r(T-t)} \left(\frac{m_t}{y_t} \right)^{2r/\sigma^2} \Phi(-a_3) \right),$$

where $m_t := \inf_{0 \leq u \leq t} X_u$, and

$$a_1 = \frac{\log(X_t/m_t) + (r + \sigma^2/2)(T-t)}{\sigma\sqrt{T-t}}, \quad a_2 = a_1 - \sigma\sqrt{T-t} \text{ and } a_3 = a_1 - \frac{2r}{\sigma}\sqrt{T-t}.$$

In the meantime, the option price Y_t can also be represented as a solution to the following BSDE,

$$\begin{cases} dY_t = rY_t dt + Z_t dW_t, \\ Y_T = X_T - \inf_{0 \leq t \leq T} X_t. \end{cases}$$

Therefore, we are able to apply our numerical method, and compare solutions with the true solution, and solutions from other numerical schemes.

In this example, we choose the following parameters in simulation, $x_0 = 1, \sigma = 1, r = 0.01, T = 1, m = 3$. In Figure 1, we compare the convergence of lookback option prices from different methods, and different time discretization steps. Vanilla-LSTM refers to the algorithm that the inputs to the neural networks are the stock prices. PDGM from [37] is a numerical scheme based on recurrent neural network, and it is used to solve PPDEs. LogSig-LSTM and Sig-LSTM refer to the two numerical algorithms proposed in this study. Figure 2 list all computation errors over different methods and time steps respectively.

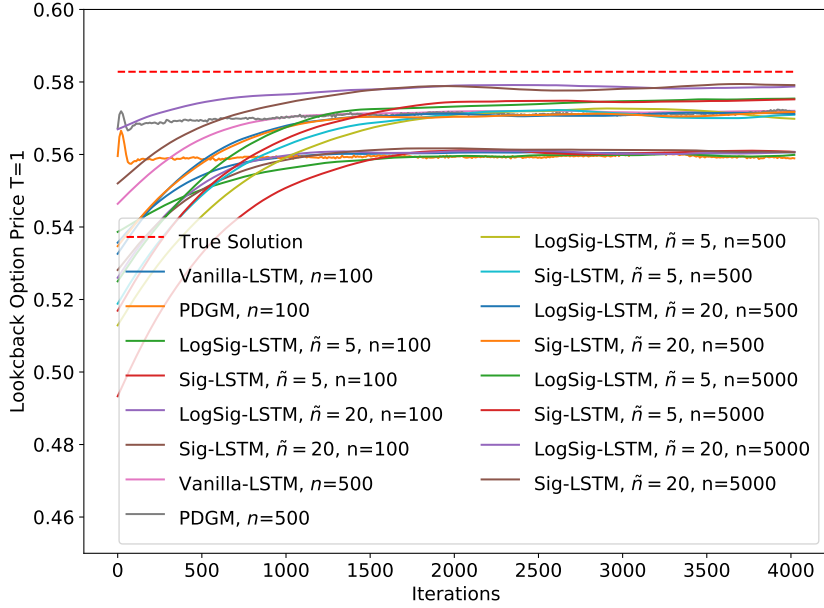


Figure 1: Convergence on lookback option prices ($T = 1$) via different methods.

The first observation is that under the same number of time steps, the numerical solutions from all methods are very similar. Secondly, the key to improve the numerical solutions to be closer to the true solution is the number of the time steps during simulation, which is quite intuitive. As we can see in Figure 2, the numerical error goes down with smaller the mesh sizes. In particular, with $n = 5000$, our log-signature and signature perform the best, and with $\tilde{n} = 20$, the numerical solution is only approximately 0.6% apart from the true solution. The third observation is that the convergence rate is slower with smaller

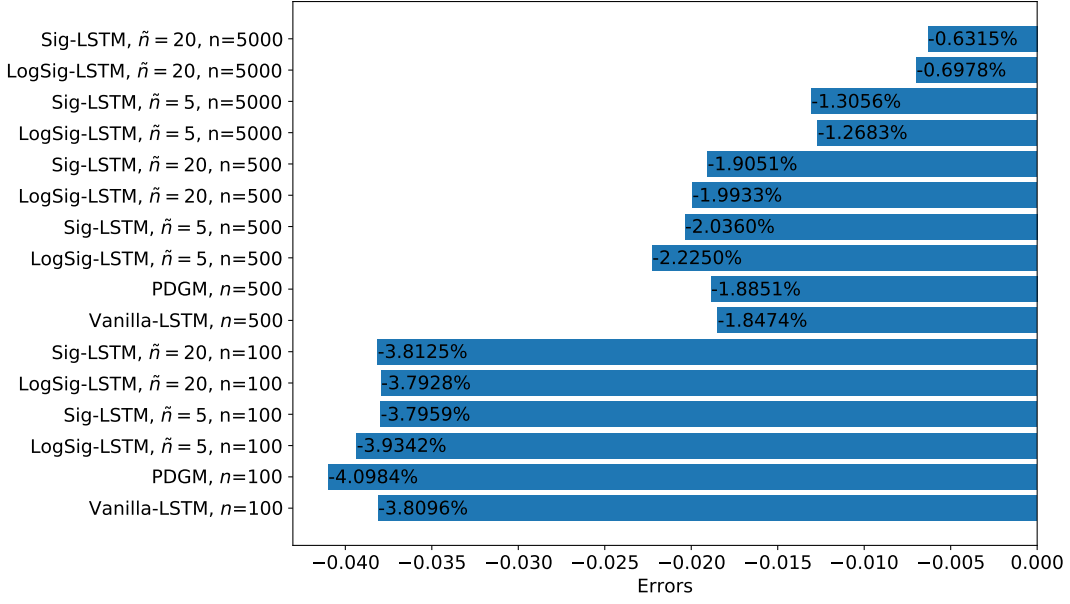


Figure 2: Option pricing errors across different methods and time steps.

number of segmentations \tilde{n} in log-signature and signature method. In addition, with a larger number of segmentations, the numerical results are generally better. Therefore, one may be encouraged to have n become as large as possible. However, this is not feasible in practice due to the running times.

Figure 3 compares the running times over different methods and time steps respectively. The running times are approximately linear with the number of segmentations and time steps. Log-signature and signature methods run 100 times faster with 5 segmentation ($\tilde{n} = 5$) than vanilla-LSTM with 500 times steps ($n = 500$). Therefore, summarizing the stock data paths into signature into a few segmentations, and then inputting them into the neural network would save us a great amount of time, and obtain the similar accuracy.

In addition, our method can handle high-frequency data. It would be impracticable to input a stock paths with $n = 5000$ into the vanilla-LSTM since it would take too long to train. However, we could first divide the 5000 time steps into 5 or 20 segmentation, and then compute the log-signature and signature of segmentations, which will be finally input into the neural networks. As we can see from this example, our method reaches a higher accuracy in an time efficient manner.

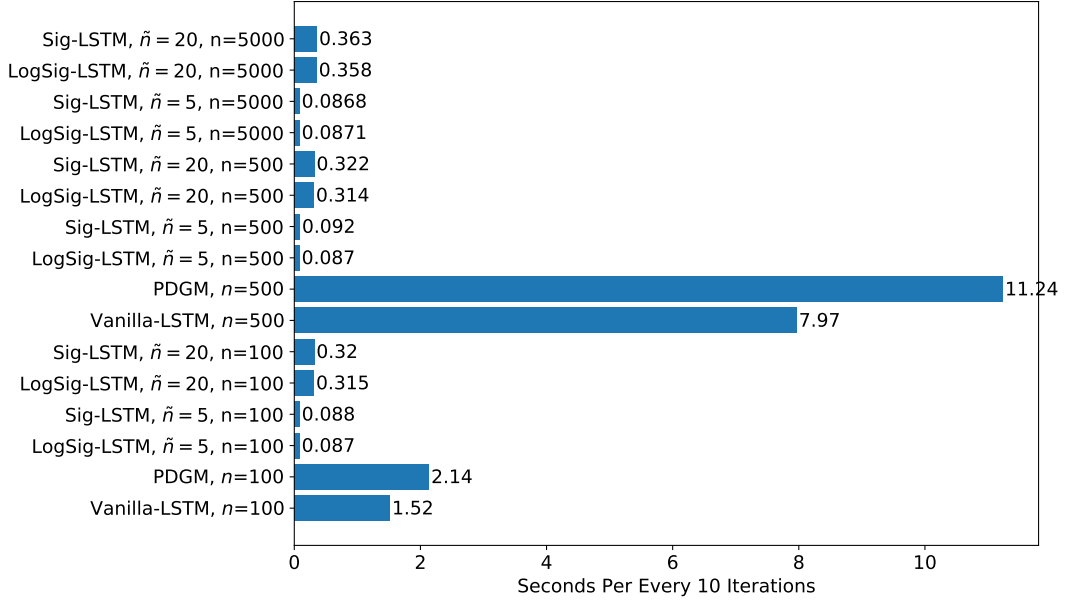


Figure 3: Computation times over different methods and time steps.

Furthermore, our method could handle high frequency data with a long time duration. In general, for a given time horizon T , we could choose n (e.g. $n=5000$ or larger) large enough such that we can still simulate the asset dynamic with small step size, i.e. Δt small, while the number of segments remain fixed. In our algorithm, the time discretization n will only affect the data generation process which is offline. The computation efficiency of our algorithm is only affected by the number of segments \tilde{n} . Continuing with lookback option example, now we choose the parameters to be $x_0 = 1, r = 0.01, \sigma = 0.05, T = 10$. Since the numerical difference between log-signature and signature methods are minimal, we only make a comparison between vanilla-LSTM and Sig-LSTM in Figure 4. Figure 5 plots a closeup of lookback option prices with different time-steps. Comparing to Vanilla-LSTM with $n = 500$, our Sig-LSTM methods with $\tilde{n} = 5$ and $n = 5000$ improves the accuracy by 1.36%, and underestimates the solution only 0.624%. In the meantime, our Sig-LSTM method with $\tilde{n} = 5$ and $n = 5000$ runs 100 times faster than Vanilla-LSTM with $n = 500$.

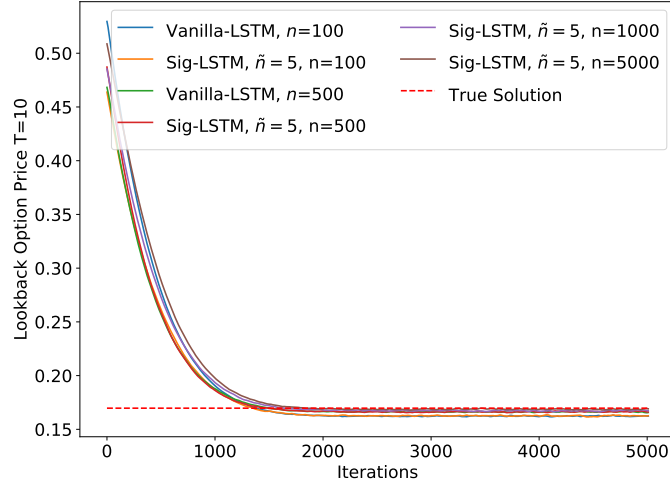


Figure 4: High frequency long duration lookback option pricing example ($T = 10$).

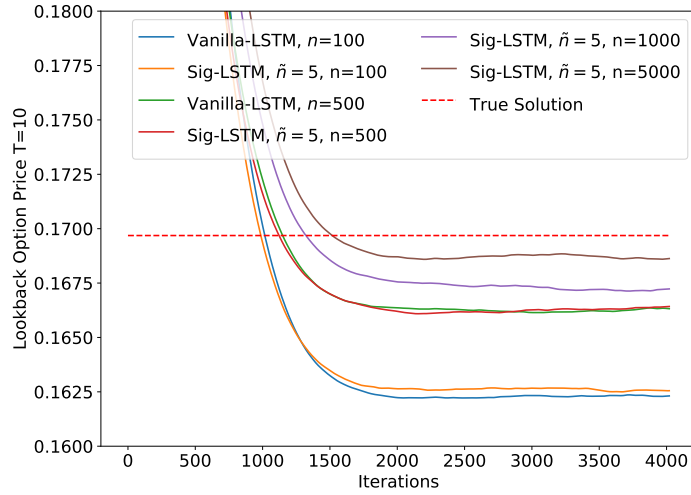


Figure 5: High frequency long duration lookback option pricing example ($T = 10$ zoomed plot).

3.3 European Call Option in the Heston Model under Parameter Uncertainty

We consider the Heston model in [10] for a European call option pricing problem with stochastic volatility model under parameter uncertainty. For $t \in [0, T]$, the asset price S and forward variance process V follows,

$$\begin{cases} dS_t = rS_t dt + \sqrt{V_t}S_t(\rho dW_t^1 + \sqrt{1-\rho^2}dW_t^2), \\ dV_t = (\kappa\theta - [\kappa + \sigma\lambda]V_t)dt + \sigma\sqrt{V_t}dW_t^1, \end{cases}$$

and W^1, W^2 are two Brownian motions under the risk neutral measure \mathbb{Q} with correlation $\rho \in (-1, 1)$. Parameters (κ, θ, σ) are assumed to be nonnegative and satisfy the Feller's condition $2\kappa\theta \geq \sigma^2$ to guarantee that variance process V is bounded below from zero. Moreover, under the parameter uncertainty situation, an elliptical uncertainty set for parameters (r, κ, β) , where $\beta \equiv \kappa\theta$ with $(1 - \alpha)$ confidence is given by the quadratic form $U = \{u : u^T \Sigma_{r, \kappa, \beta}^{-1} u \leq \chi\}$, where u is the perspective deviance towards the true parameters denoted as $u_t = (r_t - r, \kappa_t - \kappa, \beta_t - \beta)$, $\Sigma_{r, \kappa, \beta}^{-1}$ is the covariance matrix of the parameters and $\chi := \chi_3^2(1 - \alpha)$ is the quantile of the chi-square distribution with three degrees of freedom. We should remark here that ellipsoidal specifications of uncertainty appear naturally in multivariate Gaussian settings for the uncertainty about the drifts of tradeable asset prices, and literature can be referred to [3, 4, 16]. In [10], the pricing bound for the Heston call option under model ambiguity is derived and proved to be the unique solutions of the following BSDEs with payoff $g(S_T) = (S_T - K)^+$ at maturity T ,

$$\begin{cases} dY_t^\pm = -H^\pm(S_t, V_t, Y_t^\pm, Z_t)dt + Z_t dW_t, & Y_T^\pm = g(S_T), \\ H^\pm(S_t, V_t, Y_t^\pm, Z_t) = \pm \sqrt{\chi \eta_t^T \Sigma^T \eta_t} - rY_t, \end{cases} \quad (3.15)$$

where $\eta_t \in \mathbb{R}^{3 \times 1}$ is the vector of coefficients to the parameter deviances of equation given by

$$\eta_t = \left[\left(\frac{Z_t^2}{\sqrt{1-\rho^2}\sqrt{V_t}} - Y_t \right), \left(\frac{-Z_t^1 \sqrt{V_t}}{\sigma} + \frac{\rho Z_t^2 \sqrt{V_t}}{\sigma \sqrt{1-\rho^2}} \right), \left(\frac{Z_t^1}{\sigma \sqrt{V_t}} - \frac{\rho Z_t^2}{\sigma \sqrt{1-\rho^2}\sqrt{V_t}} \right) \right]^T,$$

and $Z_t, W_t \in \mathbb{R}^2$. Also, the perspective deviance towards the true parameter corresponding to (3.15) are $u^\pm(S_t, V_t, Y_t^\pm, Z_t) = \pm \sqrt{\frac{\chi}{\eta_t^T \Sigma^T \eta_t}} \Sigma \eta_t$. Following the idea in [10], the forward

component $X = (S, V)$ of the SDE is generated by standard Euler-Maruyama scheme for the log-price and an implicit Milstein scheme for the variance

$$\begin{cases} \log S_t^\pi = \log S_{t_{i-1}}^\pi + (r - \frac{1}{2}V_{t_{i-1}}^\pi)\Delta_i + \sqrt{V_{t_{i-1}}^\pi}(\rho\Delta W_{t_i}^1 + \sqrt{1-\rho^2}\Delta W_{t_{i-1}}^2), \\ V_{t_i}^\pi = \frac{V_{t_{i-1}}^\pi + \kappa\theta\Delta_i + \sigma\sqrt{V_{t_{i-1}}^\pi}\Delta W_{t_i}^2 + \frac{1}{4}\sigma^2((\Delta W_{t_i}^2)^2 - \Delta_i)}{1 + \kappa\Delta_i}, \end{cases}$$

where $\Delta W_{t_i}^1, \Delta W_{t_i}^2$ are independent variables generated from the zero-mean normal distribution with variance Δ_i .

We implement the example in [10] with the same experiment set up: $S_0 = 100$, $V_0 = 0.0457$, $r = 0.05$, $\kappa = 5.070$, $\theta = 0.0457$, $\sigma = 0.4800$, $\rho = -0.767$, $K = 100$, $T = 1$, and covariance matrix $\Sigma = \text{Diag}(2.5e-05, 0.25, 1e-04) \in \mathbb{R}^{3 \times 3}$.

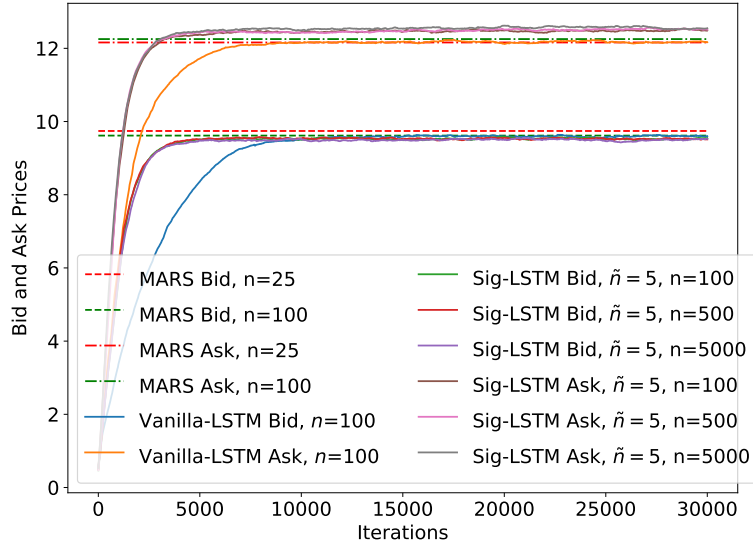


Figure 6: A better bound for bid and ask prices.

From Figure 6, we can see that our method provides a better pricing bound over the recursive MARS degree 2 with variance reduction method (denoted as “MARS” in the figure) in [10], by providing a slightly wider bound for the optimally controlled value process. The zoomed plots are in Figure 7 and 8. As we increase the number of time steps to $n = 200$, the Vanilla-LSTM performs better than MARS method with $n = 25$, and $n = 100$. Lastly,

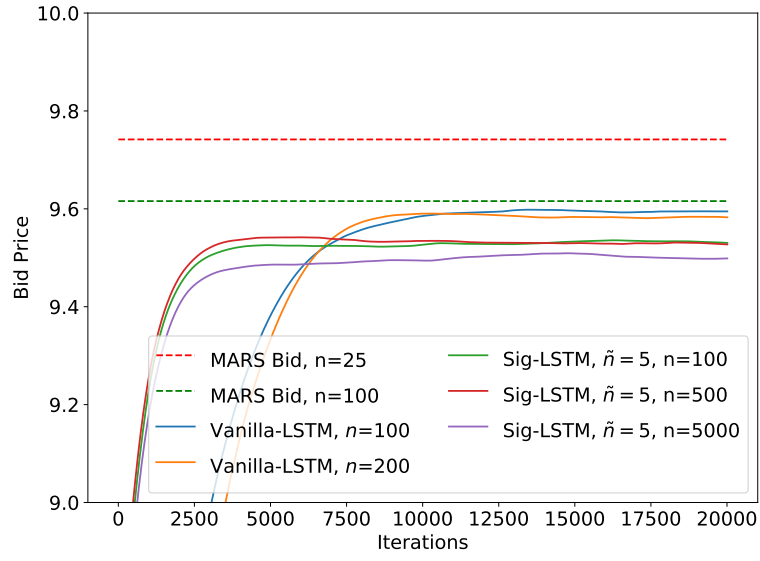


Figure 7: Zoomed plots for bid prices.

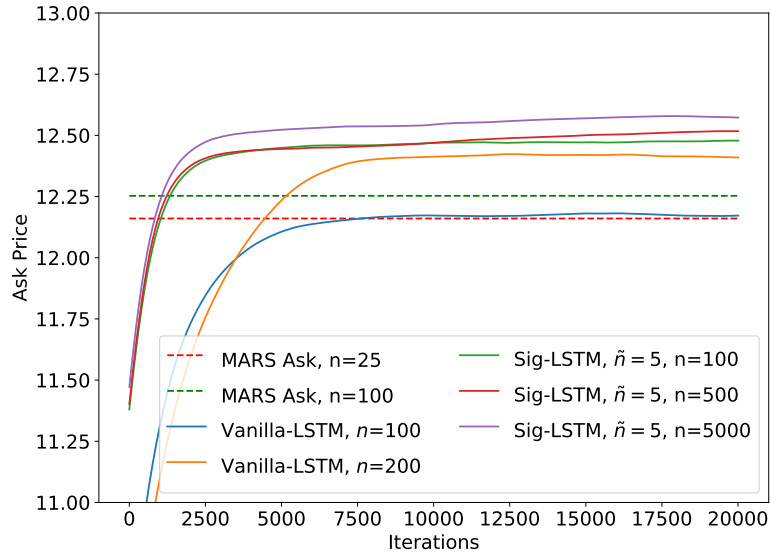


Figure 8: Zoomed plots for ask prices.

with $\tilde{n} = 5$, and $n = 5000$, our Sig-LSTM method efficiently improves the bound. This is what we should expect. With a larger number of time discretization n , the driver H^\pm in (3.15) are updated more accurately, which leads to the value process Y^\pm in (3.15) optimised to a higher degree.

Table 2: Bid ask prices for European call under Heston model

MARS Bid $n = 25$	MARS Bid $n = 100$	Vanilla-LSTM Bid $n = 100$	Vanilla-LSTM Bid $n = 200$	Sig-LSTM Bid $\tilde{n} = 5, n = 100$	Sig-LSTM Bid $\tilde{n} = 5, n = 500$	Sig-LSTM Bid $\tilde{n} = 5, n = 5000$
9.74	9.62	9.59	9.58	9.53	9.527	9.50
MARS Ask $n = 25$	MARS Ask $n = 100$	Vanilla-LSTM Ask $n = 100$	Vanilla-LSTM Ask $n = 200$	Sig-LSTM Ask $\tilde{n} = 5, n = 100$	Sig-LSTM Ask $\tilde{n} = 5, n = 500$	Sig-LSTM Ask $\tilde{n} = 5, n = 5000$
12.16	12.25	12.17	12.41	12.48	12.52	12.57

3.4 A High Dimensional Example

In this section, we consider the following path-dependent BSDE,

$$Y_t = g(X_{[0,T]}) + \int_t^T f(s, X_\cdot, Y_s, Z_s) ds - \int_t^T Z_s dB_s, \quad (3.16)$$

and the forward process is given by $dX_t = dB_t$, $X_0 = 0$. Based on the association with PPDE and the nonlinear Feynman-Kac formula, we construct a high dimensional example, which we could find the true solution. For simplicity, we choose

$$f = 0, \quad \text{and} \quad g(X_\cdot) = \left(\int_0^T \sum_{i=1}^d X_s^i ds \right)^2.$$

We then compare the true solution with the solution approximated by our algorithm. In this example, we use the deep log-signature BSDE algorithm because the input of the network grows exponentially in terms of the dimension. By applying the log-signature layer, we could potentially solve higher dimension problems. With $d = 20, T = 1, \tilde{n} = 5, n = 100$, after 10000 training iteration, the approximated solution of Y_0 from our algorithm is 6.60 with an error of 1% to the true solution of 6.66. Again, our algorithm runs only 5 steps ($\tilde{n} = 5$) during training, which is quite time efficient. Here we remark that even our algorithm is able to approximate the true solution of the high dimensional example, it is more suitable for high frequency, path dependent and long duration data. This is because when generating signatures / log-signatures from high dimensional paths, the dimension of signatures / log-signatures would increase exponentially in terms of the dimension of the path, we could see this from equation (2.2).

We present the equivalent PPDE of our path-dependent BSDE example in (3.16). The setup and definition of path derivatives can be found in Subsection 4.2. On the canonical space $([0, T] \times C([0, T], \mathbb{R}^d))$, the PPDE follows

$$\begin{cases} \partial_t u + \frac{1}{2} \text{tr}(\partial_{\omega\omega} u) + f(t, \omega, u, \partial_{\omega} u) = 0, \\ u(T, \omega) = \xi(\omega). \end{cases}$$

For this high dimensional example with generator $f = 0$, and terminal condition $\xi(\omega) = \left(\int_0^T \sum_{i=1}^d \omega_s^i ds\right)^2$, the PPDE yields an explicit solution

$$u(t, \omega) = \left(\int_0^t \sum_{i=1}^d \omega_s^i ds\right)^2 + \left(\sum_{i=1}^d \omega_t^i\right)^2 (T-t)^2 + 2(T-t) \left(\sum_{i=1}^d \omega_t^i\right) \int_0^t \sum_{i=1}^d \omega_s^i ds + \frac{d}{3}(T-t)^3.$$

3.5 Another Nonlinear Example

In this example, we apply our algorithm to approximate the solutions of a non-linear FBSDE (3.16) with $d = 1$, and the generator is

$$\begin{aligned} f(t, X_{[0,t]}, Y_t, Z_t) = & -\left(\min_{\mu \in [\underline{\mu}, \bar{\mu}]} \mu Z_t + \max(\sin(X_t + \int_0^t X_s ds), 0)(\bar{\mu} + X_t) \right. \\ & \left. + \min(\sin(X_t + \int_0^t X_s ds), 0)(\underline{\mu} + X_t) + \frac{1}{2} \cos(X_t + \int_0^t X_s ds) \right) \end{aligned} \quad (3.17)$$

In the numerical implementation, we choose the terminal condition to be $Y_T = \cos(X_T + \int_0^T X_s ds)$, and the forward asset process $dX_t = dB_t$. The solution is explicitly given by $Y_t = \cos(X_t + \int_0^t X_s ds)$. This example is inspired by a two person zero sum game from [33]. We choose the following parameters to implement our algorithm: $X_0 = 0$, $\underline{\mu} = 0.2$, $\bar{\mu} = 0.3$, $T = 1$. As illustrated in Figure 9 and Table 3, with an increase of number of segmentation \tilde{n} and number of time steps n in the Euler scheme will simultaneously improve the accuracy. With only 20 segmentations ($\tilde{n} = 20$) for $n = 1000$, Y_0 reaches 0.9982 with an error of only 0.18%, where true solution is 1.

Table 3: Y_0 in the Nonlinear Example

	$\tilde{n} = 5$	$\tilde{n} = 20$	$\tilde{n} = 50$	$\tilde{n} = 100$
$n = 100$	0.986	0.9979	0.9988	—
$n = 1000$	0.987	0.9982	0.9991	0.9997

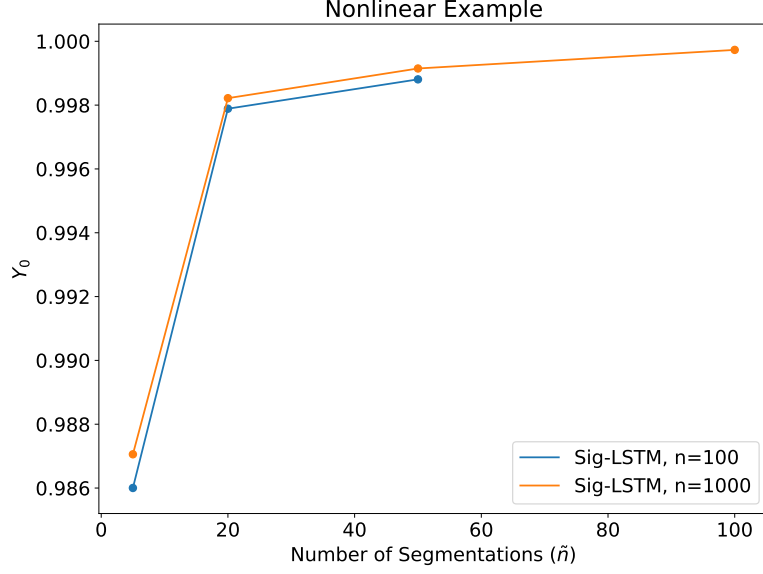


Figure 9: Nonlinear Example.

For this non-linear example, the equivalent PPDE follows

$$\begin{cases} \partial_t u + \frac{1}{2} \partial_{\omega\omega} u + \min_{\mu \in [\underline{\mu}, \bar{\mu}]} \mu \partial_{\omega} u + f_0(t, \omega, \bar{\omega}) = 0 \\ u(T, \omega) = g(\omega_T, \bar{\omega}_T), \end{cases} \quad (3.18)$$

where $g(\omega_T, \bar{\omega}_T) = \cos(\omega_T + \bar{\omega}_T)$, and $\bar{\omega}_t := \int_0^t \omega_s ds$, and

$$f_0(t, \omega, \bar{\omega}) = \max(\sin(\omega_t + \bar{\omega}_t), 0)(\bar{\mu} + \omega_t) + \min(\sin(\omega_t + \bar{\omega}_t), 0)(\underline{\mu} + \omega_t) + \frac{1}{2} \cos(\omega_t + \bar{\omega}_t).$$

4 Convergence analysis

In this section, we study the universality approximation property of the Markov FBSDE (2.5) and the non-Markovian FBSDE (2.6) by using the deep (log) signature and DNN in the standard Euler schemes. For notation simplicity, we may carry out the proofs only for one-dimensional case, i.e. $d = d_1 = d_2 = 1$. Before we show the main estimates, we first introduce the following universality property for neural network from [15], see also [23].

Lemma 4.1. *Let $\hat{\sigma}(x)$ be a sigmoid function (i.e. a non-constant, increasing, and bounded continuous function on \mathbb{R}). Let K be any compact subset of \mathbb{R}^n , and $\hat{f} : K \rightarrow \mathbb{R}^d$ be a continuous function mapping. Then for an arbitrary $\varepsilon > 0$, there exists an integer $N > 0$, an $d \times N$ matrix A and an N dimensional vector θ such that*

$$\max_{x \in K} |\hat{f}(x) - A\hat{\sigma}(Bx + \theta)| \leq \varepsilon,$$

holds where $\hat{\sigma} : \mathbb{R}^N \rightarrow \mathbb{R}^d$ is a sigmoid mapping defined by

$$\hat{\sigma}(' (u_1, \dots, u_N)) = ' (\hat{\sigma}(u_1), \dots, \hat{\sigma}(u_N)).$$

where $'(u_1, \dots, u_N)$ denotes the permutation of the sequence (u_1, \dots, u_N) .

For the time horizon $[0, T]$, we denote $h := (T - t)/n$ as the step size for the standard Euler scheme, and we denote $t_i := ih, i = 0, \dots, n$. Similarly, for some $k \in \mathbb{R}^+$, we denote $u := k \times (T - t)/n$ as the step size for the deep signature Euler scheme, and we denote $u_i := iu = ikh$, with $\Delta u_i = u_i - u_{i-1} = kh$, for $i = 0, \dots, n/k := \tilde{n}$. Furthermore, we keep the convention that $\Delta W_{i+1} := W_{i+1} - W_i$ and $\Delta W_{u_{i+1}} := W_{u_{i+1}} - W_{u_i}$.

4.1 Markovian case

According to deep signature Euler scheme (2.10), we have

$$Y_{u_i}^{\tilde{n}, \text{Sig}} := Y_{u_{i-1}}^{\tilde{n}, \text{Sig}} - f(u_{i-1}, X_{u_{i-1}}^n, Y_{u_{i-1}}^{\tilde{n}, \text{Sig}}, Z_{u_{i-1}}^{\theta, \text{Sig}}) \Delta u_i + Z_{u_{i-1}}^{\theta, \text{Sig}} \Delta W_{u_i}.$$

where $Z_{u_i}^{\theta, \text{Sig}} := \mathcal{R}^\theta(\pi_m(\text{Sig}(X^n)_0), \dots, \pi_m(\text{Sig}(X^n)_{i-1}))$. At last, we denote $Y_{u_i}^n$ and $Z_{u_i}^n$ as values for the standard Euler scheme approximation of Y and Z (equation (2.5)) at time u_i . The following estimate is a standard result for Markov BSDEs, see [40][Theorem 5.3.3].

Lemma 4.2. *Let Assumptions 1 hold and assume h is small enough. Then*

$$\max_{0 \leq i \leq n} \mathbb{E} \left[\sup_{t_i \leq t \leq t_{i+1}} |Y_t - Y_{t_i}|^2 \right] + \sum_{i=0}^{n-1} \mathbb{E} \left[\int_{t_i}^{t_{i+1}} |Z_t - Z_{t_i}|^2 dt \right] \leq C[1 + |x|^2]h.$$

With the above lemma in hand, we are ready to prove the universal approximation property.

Proof [Proof of Lemma 2.4] We assume that constant C changes generically from line to line. Applying the triangle inequality, for $t \in [u_i, u_{i+1}]$, we have

$$|Z_t - Z_{u_i}^{\theta, \text{Sig}}|^2 \leq 2[|Z_t - Z_{u_i}|^2 + |Z_{u_i} - Z_{u_i}^{\theta, \text{Sig}}|^2],$$

which implies

$$\sum_{i=0}^{\tilde{n}-1} \mathbb{E} \left[\int_{u_i}^{u_{i+1}} |Z_t - Z_{u_i}^{\theta, \text{Sig}}|^2 dt \right] \leq 2 \left\{ \sum_{i=0}^{\tilde{n}-1} \mathbb{E} \left[\int_{u_i}^{u_{i+1}} |Z_t - Z_{u_i}|^2 dt + \int_{u_i}^{u_{i+1}} |Z_{u_i} - Z_{u_i}^{\theta, \text{Sig}}|^2 dt \right] \right\}.$$

By Lemma (4.2), we can obtain that

$$\sum_{i=0}^{\tilde{n}-1} \mathbb{E} \left[\int_{u_i}^{u_{i+1}} |Z_t - Z_{u_i}|^2 dt \right] \leq C(1 + |x|^2)kh \leq C(1 + |x|^2)\delta.$$

Furthermore, since $\tilde{n} \times kh = T$, we observe that

$$\sum_{i=0}^{\tilde{n}-1} \mathbb{E} \left[\int_{u_i}^{u_{i+1}} |Z_{u_i} - Z_{u_i}^{\theta, \text{Sig}}|^2 dt \right] \leq T \max_{0 \leq i \leq \tilde{n}-1} \mathbb{E}[|Z_{u_i} - Z_{u_i}^{\theta, \text{Sig}}|^2].$$

Now it suffices to show that for any ε , there exists network θ such that $\max_{0 \leq i \leq \tilde{n}-1} \mathbb{E}[|Z_{u_i} - Z_{u_i}^{\theta, \text{Sig}}|^2] \leq \varepsilon/2T$. From the non-linear Feynman-Kac formula, we know

$$Z_t = \partial_x u \sigma(t, X_t) := \mathcal{F}(t, X_t).$$

For simplicity, we further assume that the solution $u \in \mathcal{C}_b^{\infty, \infty}$ and $\sigma \in \mathcal{C}_b^\infty$, which implies that $\mathcal{F} \in \mathcal{C}_b^{\infty, \infty}$. We thus have the following Taylor expansion,

$$dZ_t = d\mathcal{F}(t, X_t) = \partial_t \mathcal{F}(t, X_t)dt + \partial_x \mathcal{F}(t, X_t) \circ dX_t. \quad (4.19)$$

Applying the change of variable formula iteratively, we get the following local approximation by using Taylor expansion at step N ,

$$Z_t - Z_s = \mathcal{F}(t, X_t) - \mathcal{F}(s, X_s) \approx \sum_{k=1}^N \mathcal{F}^{\circ k}(\widehat{X}_s) \int_{I_k} \circ d\widehat{X}_{t_1} \otimes \cdots \otimes d\widehat{X}_{t_k} \quad (4.20)$$

where we denote $I_k := \{s < t_1 < t_2 < \cdots < t_k < t\}$ as the subdivision of the time interval $[s, t]$, and $\{\widehat{X}_t\}_{t \in [0, T]} := \{t, X_t\}_{t \in [0, T]}$ as the enhanced path of the time parameter and the path $\{X_t\}_{t \in [0, T]}$. The coefficient term $\mathcal{F}^{\circ k}$ in the above Taylor expansion is defined recursively,

$$\mathcal{F}^{\circ 1} = \mathcal{F} =: \partial_x u \sigma, \quad \mathcal{F}^{\circ k+1} = D(\mathcal{F}^{\circ k}),$$

where D denotes the differential operator. Following the idea in [23][Section 4], we consider the step- N Taylor expansion of Z , denoted as $\{\hat{Z}_{u_i}\}_{i=0}^{\tilde{n}}$. We have the following approximation of Z_{u_i} ,

$$\begin{aligned} Z_{u_i} = \mathcal{F}(u_i, X_{u_i}) &\approx \hat{Z}_{u_i} = \hat{Z}_{u_{i-1}} + \sum_{k=1}^N \mathcal{F}^{ok}(\hat{X}_{u_{i-1}}) \hat{X}_{u_{i-1}, u_i}^k \\ &= g_N^{\mathcal{F}}(\text{Sig}_{u_{i-1}}, \hat{Z}_{u_{i-1}}), \\ \text{or} \quad &= \tilde{g}_N^{\mathcal{F}}(\text{LS}_{u_{i-1}}, \hat{Z}_{u_{i-1}}), \end{aligned}$$

where $\text{LS}_{u_{i-1}}$ is the log-signature layer of \hat{X} , and $\text{Sig}_{u_{i-1}}$ is the signature layer of \hat{X} . Plugging in $Z_{u_i}^{\theta, \text{Sig}} = \mathcal{R}^\theta((\text{Sig}_k)_{k=0}^{u_{i-1}})$ (or $Z_{u_i}^{\theta, \text{LS}} = \mathcal{R}^\theta((\text{LS}_k)_{k=0}^{u_{i-1}})$), for any u_i , we have

$$\begin{aligned} |Z_{u_i} - Z_{u_i}^{\theta, \text{Sig}}| &\leq |Z_{u_i} - \hat{Z}_{u_i}| + |\hat{Z}_{u_i} - Z_{u_i}^{\theta, \text{Sig}}| \\ &\leq |Z_{u_i} - \hat{Z}_{u_i}| + |g_N^{\mathcal{F}}(\text{Sig}_{u_{i-1}}, \hat{Z}_{u_{i-1}}) - Z_{u_i}^{\theta, \text{Sig}}| \\ \text{or} \quad |Z_{u_i} - Z_{u_i}^{\theta, \text{LS}}| &\leq |Z_{u_i} - \hat{Z}_{u_i}| + |\tilde{g}_N^{\mathcal{F}}(\text{LS}_{u_{i-1}}, \hat{Z}_{u_{i-1}}) - Z_{u_i}^{\theta, \text{Sig}}|. \end{aligned}$$

Applying Lemma 4.1, for any $\varepsilon > 0$, as long as $kh = T/\tilde{n}$ is small enough and the truncation order of the signature is large enough, we can always find a θ such that $\max_{i=0}^{\tilde{n}-1} \mathbb{E}[|Z_{u_i} - Z_{u_i}^{\theta, \text{Sig}}|^2] \leq \varepsilon/2T$, for any given T . In particular, ε is independent of time discretization. If we replace the signature with log-signature, the proof follows similarly. (A similar proof for forward SDE can be found in [23][Theorem 4.1]). \blacksquare

Proof [Proof of Theorem 2.5] Applying triangle inequality, we have

$$|Y_t - Y_{u_i}^{\tilde{n}, \text{Sig}}|^2 \leq C[|Y_t - Y_{u_i}|^2 + |Y_{u_i} - Y_{u_i}^{\tilde{n}, \text{Sig}}|^2].$$

According to Lemma 4.2, one can obtain that

$$\max_{0 \leq i \leq \tilde{n}} \mathbb{E}[\sup_{u_i \leq t \leq u_{i+1}} |Y_t - Y_{u_i}|^2] \leq C(1 + |x|^2)kh \leq C(1 + |x|^2)\delta. \quad (4.21)$$

Next, it suffices to show that $\max_{0 \leq i \leq \tilde{n}} \mathbb{E}[|Y_{u_i} - Y_{u_i}^{\tilde{n}, \text{Sig}}|^2] \leq C(1 + |x|^2)kh$. We denote $\Delta Y_{u_i}^{\tilde{n}, \text{Sig}} := Y_{u_i} - Y_{u_i}^{\tilde{n}, \text{Sig}}$, and $I_t^{u_i} := f(t, X_t, Y_t, Z_t) - f(u_i, X_{u_i}, Y_{u_i}^{\tilde{n}, \text{Sig}}, Z_{u_i}^{\theta, \text{Sig}})$. We thus have

$$\Delta Y_{u_{i+1}}^{\tilde{n}, \text{Sig}} = \Delta Y_{u_i}^{\tilde{n}, \text{Sig}} - \int_{u_i}^{u_{i+1}} I_t^{u_i} dt + \int_{u_i}^{u_{i+1}} Z_t - Z_{u_i}^{\theta, \text{Sig}} dW_t.$$

Taking squares on both sides and taking expectation, we have

$$\mathbb{E}[|\Delta Y_{u_{i+1}}^{\tilde{n}, \text{Sig}}|^2] \leq C\mathbb{E}\left[|\Delta Y_{u_i}^{\tilde{n}, \text{Sig}}|^2 + \int_{u_i}^{u_{i+1}} |I_t^{u_i}|^2 dt + \int_{u_i}^{u_{i+1}} |Z_t - Z_{u_i}^{\theta, \text{Sig}}|^2 dt\right].$$

According to Assumption 1, we further conclude that

$$\begin{aligned}
|I_t^{u_i}|^2 &\leq |f(t, X_t, Y_t, Z_t) - f(u_i, X_{u_i}, Y_{u_i}, Z_{u_i})|^2 \\
&\quad + |f(u_i, X_{u_i}, Y_{u_i}, Z_{u_i}) - f(u_i, X_{u_i}, Y_{u_i}^{\tilde{n}, \text{Sig}}, Z_{u_i}^{\theta, \text{Sig}})|^2 \\
&\leq L[(kh)^2 + |Y_t - Y_{u_i}|^2 + |X_t - X_{u_i}|^2 + |Z_t - Z_{u_i}|^2 \\
&\quad + |\Delta Y_{u_i}^{\tilde{n}, \text{Sig}}|^2 + |Z_{u_i} - Z_{u_i}^{\theta, \text{Sig}}|^2].
\end{aligned} \tag{4.22}$$

Plugging (4.22) into previous estimates, we obtain

$$\begin{aligned}
\mathbb{E}\left[\int_{u_i}^{u_{i+1}} |I_t^{u_i}|^2 dt\right] &\leq \mathbb{E}\left[L \int_{u_i}^{u_{i+1}} |Y_t - Y_{u_i}|^2 + |X_t - X_{u_i}|^2 + |Z_t - Z_{u_i}|^2 dt \right. \\
&\quad \left. + L(kh)^3 + Lkh|\Delta Y_{u_i}^{\tilde{n}, \text{Sig}}|^2 + Lkh|Z_{u_i} - Z_{u_i}^{\theta, \text{Sig}}|^2\right].
\end{aligned}$$

Applying Lemman 4.2 and Lemma 2.4, we further get the following estimates

$$\begin{aligned}
\mathbb{E}\left[\int_{u_i}^{u_{i+1}} |I_t^{u_i}|^2 dt\right] &\leq C(1 + |x|^2)kh + L(kh)^2 + Lkh\varepsilon + Lkh\mathbb{E}[|\Delta Y_{u_i}^{\tilde{n}, \text{Sig}}|^2] \\
&\leq C(1 + |x|^2 + \varepsilon)kh + Lkh\mathbb{E}[|\Delta Y_{u_i}^{\tilde{n}, \text{Sig}}|^2].
\end{aligned}$$

Combining the above estimates and Lemma 2.4, for some constants C_1 and C_2 , we have

$$\mathbb{E}[|\Delta Y_{u_{i+1}}^{\tilde{n}, \text{Sig}}|^2] \leq C_1\mathbb{E}[|\Delta Y_{u_i}^{\tilde{n}, \text{Sig}}|^2] + C_2(1 + |x|^2 + \varepsilon)kh. \tag{4.23}$$

Then by (4.23) and Grönwall's inequality, we can conclude that

$$\max_{0 \leq i \leq \tilde{n}} \mathbb{E}[|Y_{u_i} - Y_{u_i}^{\tilde{n}, \text{Sig}}|^2] \leq C(1 + |x|^2 + \varepsilon)kh. \tag{4.24}$$

At last, combining (4.21) and (4.24), we have

$$\max_{0 \leq i \leq \tilde{n}} \mathbb{E}\left[\sup_{u_i \leq t \leq u_{i+1}} |Y_t - Y_{u_i}^{\tilde{n}, \text{Sig}}|^2\right] \leq C[1 + |x|^2 + \varepsilon]\delta.$$

■

4.2 Non-Markovian case

We first introduce the following notations (see e.g. [11]). Let $T > 0$ be fixed. Denote $\Omega := \{\omega \in C([0, T], \mathbb{R}^d)\}$ as the canonical space, and denote $\Lambda := [0, T] \times \Omega$. For simplification,

we still consider $d = 1$ below. For each $\omega \in \Omega$, $X : \Lambda \rightarrow \mathbb{R}$ is the canonical process, namely $X_t(\omega) := \omega_t$. For each $t < t'$ and $(t, \omega), (t', \omega') \in \Lambda$, we denote

$$\|\omega\|_t := \sup_{s \in [0, t]} |\omega_s|, \quad d_\infty((t, \omega), (t', \omega')) := \sup_{s \in [0, T]} |\omega_{s \wedge t} - \omega'_{s \wedge t'}| + |t - t'|. \quad (4.25)$$

Then $(\Omega, \|\cdot\|)$ is a Banach space, and (Λ, d_∞) is a complete pseudometric space. For a function $u : \Lambda \rightarrow \mathbb{R}$, the path derivatives of u are defined as, if they exist,

$$\begin{aligned} D_t u(t, \omega_{\cdot \wedge t}) &= \lim_{h \rightarrow 0, h > 0} \frac{1}{h} [u(t+h, \omega_{\cdot \wedge t}) - u(t, \omega_{\cdot \wedge t})], \\ D_\omega u(t, \omega_{\cdot \wedge t}) &= \lim_{h \rightarrow 0, h > 0} \frac{1}{h} [u(t, \omega_{\cdot \wedge t} + h \mathbf{1}_{[t, T]}) - u(t, \omega_{\cdot \wedge t})]. \end{aligned} \quad (4.26)$$

Similarly, we define $D_{\omega\omega} u(t, \omega_{\cdot \wedge t}) = D_\omega(D_\omega u(t, \omega_{\cdot \wedge t}))$. We first introduce the following functional Itô's formula from [11].

Theorem 4.3. *Let $(\tilde{\Omega}, \mathcal{F}, (\mathcal{F}_t)_{t \in [0, T]}, \mathbb{P})$ be a probability space, if X is a continuous semimartingale and u is in $\mathbb{C}^{1,2}(\Lambda)$, then for any $t \in [0, T]$:*

$$u(X_t) - u(X_0) = \int_0^t D_s u(X_s) ds + \int_0^t D_x u(X_s) dX_s + \frac{1}{2} \int_0^t D_{xx} u(X_s) d\langle X \rangle_s, \quad a.s.. \quad (4.27)$$

For the purpose of our analysis, we record the Stratonovich form of the above Itô's formula (4.27) as below,

$$u(X_t) - u(X_0) = \int_0^t D_s u(X_s) ds + \int_0^t D_x u(X_s) \circ dX_s. \quad (4.28)$$

Now we are ready to prove the convergence of the non-Markovian FBSDE algorithm. We first introduce the following assumption.

Assumption 2. *Let the following assumptions be in force.*

- b, σ, f, g are deterministic taking values in $\mathbb{R}^{d_1}, \mathbb{R}^{d_1 \times d}, \mathbb{R}^{d_2}, \mathbb{R}^{d_2}$, respectively; and $b(\cdot, 0), \sigma(\cdot, 0), f(\cdot, 0, 0, 0)$ and $g(0)$ are bounded.
- b, σ, f, g are C^k -smooth enough with respect to all variables $(t, x_{\cdot \wedge t}, y, z)$ for any desired $k \in \mathbb{N}_+$ and all derivatives are bounded by constant L .

We denote $\bar{Y}_{u_i}^n$ and $\bar{Z}_{u_i}^n$ as values for the standard Euler scheme approximation of Y and Z at time u_i in equation (2.6). According to Theorem 4.27, the estimate from Lemma 4.2 holds true for the standard Euler scheme of (2.6) under Assumption 2.

Lemma 4.4. *Let Assumptions 2 hold and assume h is small enough. Then*

$$\max_{0 \leq i \leq n} \mathbb{E} \left[\sup_{t_i \leq t \leq t_{i+1}} |Y_t - \bar{Y}_{t_i}|^2 \right] + \sum_{i=0}^{n-1} \mathbb{E} \left[\int_{t_i}^{t_{i+1}} |Z_t - \bar{Z}_{t_i}|^2 dt \right] \leq C[1 + |x|^2]h.$$

Next, we prove the path-dependent version of Lemma 2.4 and Theorem 2.5. ~~for~~ (2.10)

Lemma 4.5. *Let **Assumption 2** hold and assume $kh < \delta$, for any $\delta > 0$, for any given $T > 0$, for some constant $C > 0$ depending on T and L , and for any $\varepsilon > 0$, there exists recurrent neural network \mathcal{R}^θ , such that*

$$\sum_{i=0}^{\tilde{n}-1} \mathbb{E} \left[\int_{u_i}^{u_{i+1}} |Z_t - \bar{Z}_{u_i}^{\theta, \text{Sig}}|^2 dt \right] \leq C[1 + |x|^2]\delta + \varepsilon.$$

Proof According to (2.10), we have

$$\bar{Y}_{u_i}^{\tilde{n}, \text{Sig}} := \bar{Y}_{u_{i-1}}^{\tilde{n}, \text{Sig}} - f(u_{i-1}, X_{[0, u_{i-1}]}, \bar{Y}_{u_{i-1}}^{\tilde{n}, \text{Sig}}, Z_{u_{i-1}}^{\theta, \text{Sig}}) \Delta u_i + \bar{Z}_{u_{i-1}}^{\theta, \text{Sig}} \Delta W_{u_i}. \quad (4.29)$$

Similar to the proof of Lemma 2.4, we have

$$\sum_{i=0}^{\tilde{n}-1} \mathbb{E} \left[\int_{u_i}^{u_{i+1}} |Z_t - \bar{Z}_{u_i}^{\theta, \text{Sig}}|^2 dt \right] \leq 2 \left\{ \sum_{i=0}^{\tilde{n}-1} \mathbb{E} \left[\int_{u_i}^{u_{i+1}} |Z_t - \bar{Z}_{u_i}|^2 dt + \int_{u_i}^{u_{i+1}} |\bar{Z}_{u_i} - \bar{Z}_{u_i}^{\theta, \text{Sig}}|^2 dt \right] \right\}.$$

Applying Lemma (4.4), we have

$$\sum_{i=0}^{\tilde{n}-1} \mathbb{E} \left[\int_{u_i}^{u_{i+1}} |Z_t - \bar{Z}_{u_i}|^2 dt \right] \leq C(1 + |x|^2)kh \leq C(1 + |x|^2)\delta.$$

Similar to proof of Lemma 2.4, we get

$$\sum_{i=0}^{\tilde{n}-1} \mathbb{E} \left[\int_{u_i}^{u_{i+1}} |\bar{Z}_{u_i} - \bar{Z}_{u_i}^{\theta, \text{Sig}}|^2 dt \right] \leq T \max_{0 \leq i \leq \tilde{n}-1} \mathbb{E}[|\bar{Z}_{u_i} - \bar{Z}_{u_i}^{\theta, \text{Sig}}|^2].$$

Next, we show that for any ε , there exists network θ such that $\max_{0 \leq i \leq \tilde{n}-1} \mathbb{E}[|\bar{Z}_{u_i} - \bar{Z}_{u_i}^{\theta, \text{Sig}}|^2] \leq \varepsilon/2T$. Applying the nonlinear Feynman-Kac formula [32] for the non-Markovian BSDE (2.6) and using the definition (4.26), we get (e.g. [32][Proposition 3.8]),

$$Z_t = D_x u(t, X_{\cdot \wedge t}) \sigma(t, X_t) := \hat{\mathcal{F}}(t, X_{\cdot \wedge t}), \quad \text{for } X_{\cdot \wedge t} \in \Lambda.$$

According to Assumption 2, we assume that the functional $\hat{\mathcal{F}} \in \mathcal{C}_b^{\infty, \infty}$ is smooth. Applying (4.28), we thus have the following Taylor expansion,

$$dZ_t = d\hat{\mathcal{F}}(t, X_{\cdot \wedge t}) = D_t \hat{\mathcal{F}}(t, X_{\cdot \wedge t}) dt + D_x \hat{\mathcal{F}}(t, X_{\cdot \wedge t}) \circ dX_t. \quad (4.30)$$

Applying the change of variable formula iteratively, we get the following local approximation by using Taylor expansion at step N ,

$$Z_t - Z_s = \widehat{\mathcal{F}}(t, X_{\cdot \wedge t}) - \widehat{\mathcal{F}}(s, X_{\cdot \wedge s}) \approx \sum_{k=1}^N \widehat{\mathcal{F}}^{\circ k}(\widehat{X}_{\cdot \wedge s}) \int_{I_k} \circ d\widehat{X}_{t_1} \otimes \cdots d\widehat{X}_{t_k},$$

which is similar to (4.20). The key difference is that the coefficient term $\widehat{\mathcal{F}}^{\circ k}$ in the above Taylor expansion is defined recursively as below,

$$\widehat{\mathcal{F}}^{\circ 1} = \widehat{\mathcal{F}} =: D_x u \sigma, \quad \widehat{\mathcal{F}}^{\circ k+1} = D(\widehat{\mathcal{F}}^{\circ k}),$$

where the derivative is defined in (4.26) following the functional Itô's formula. Since the signature term

$$\int_{I_k} \circ d\widehat{X}_{t_1} \otimes \cdots d\widehat{X}_{t_k}, \quad \text{for } k \in \mathbb{N}_+$$

is identical to the ones in Lemma 2.4, the rest of the proof follows directly from Lemma 2.4. The proof is thus completed.

Applying the above Lemma 4.5 and following the similar proof of Theorem 2.5, we have the following estimate.

Theorem 4.6. *Let **Assumption 2** be in force. Assume that $kh < \delta$ for any small $\delta > 0$, for any given $T > 0$, for some constant $C > 0$ depending on T and L in **Assumption 2**, and for any $\varepsilon > 0$, there exists recurrent neural network \mathcal{R}^θ , such that*

$$\max_{0 \leq i \leq \tilde{n}} \mathbb{E} \left[\sup_{u_i \leq t \leq u_{i+1}} |Y_t - Y_{u_i}^{\tilde{n}, \text{Sig}}|^2 \right] \leq C[1 + |x|^2 + \varepsilon]\delta.$$

5 Conclusion

This paper aims to develop efficient algorithms to solve non-Markovian FBSDEs or equivalent PPDEs. We combine the signature/log-signature transformation together with RNN model to solve the FBSDE numerically. Our algorithms show advantages in solving path-dependent problems, high-frequency data problems, and long time duration problems, which apply to a wide range of applications in financial markets.

Acknowledgments. We would like to thank Professor Jin Ma and Professor Jianfeng Zhang for all the insightful comments.

References

- [1] I. P. Arribas. Derivatives pricing using signature payoffs. *arXiv preprint arXiv:1809.09466*, 2018.
- [2] C. Bayer, P. Friz, and J. Gatheral. Pricing under rough volatility. *Quantitative Finance*, 16(6):887–904, 2016.
- [3] D. Becherer and K. Kentia. Good deal hedging and valuation under combined uncertainty about drift and volatility. *Probability, Uncertainty and Quantitative Risk*, 2(1):13, 2017.
- [4] S. Biagini and M. Ç. Pinar. The robust merton problem of an ambiguity averse investor. *Mathematics and Financial Economics*, 11(1):1–24, 2017.
- [5] T. R. Bielecki, I. Cialenco, I. Iyigunler, and R. Rodriguez. Dynamic conic finance: Pricing and hedging in market models with transaction costs via dynamic coherent acceptability indices. *International Journal of Theoretical and Applied Finance*, 16(01):1350002, 2013.
- [6] P. Carr, H. Geman, and D. B. Madan. Pricing and hedging in incomplete markets. *Journal of financial economics*, 62(1):131–167, 2001.
- [7] A. Cherny and D. Madan. New measures for performance evaluation. *The Review of Financial Studies*, 22(7):2571–2606, 2009.
- [8] I. Chevyrev and H. Oberhauser. Signature moments to characterize laws of stochastic process. *arXiv: 1810.10971v1.*, 2018.
- [9] J. H. Cochrane and J. Saa-Requejo. Beyond arbitrage: Good-deal asset price bounds in incomplete markets. *Journal of political economy*, 108(1):79–119, 2000.
- [10] S. N. Cohen and M. Tegnér. European option pricing with stochastic volatility models under parameter uncertainty. In *International symposium on bsdes*, pages 123–167. Springer, 2017.
- [11] B. Dupire. Functional itô calculus. *Quantitative Finance*, 19(5):721–729, 2019.

- [12] Q. Feng and J. Zhang. Cubature method for volterra sdes and rough volatility model. *Preprint. arXiv: 2110.12853*, 2021.
- [13] J.-P. Fouque and Z. Zhang. Deep learning methods for mean field control problems with delay. *Frontiers in Applied Mathematics and Statistics*, 6, 2020.
- [14] P. K. Friz and N. B. Victoir. *Multidimensional stochastic processes as rough paths: theory and applications*, volume 120. Cambridge University Press, 2010.
- [15] K.-I. Funahashi and Y. Nakamura. Approximation of dynamical systems by continuous time recurrent neural networks. *Neural networks*, 6(6):801–806, 1993.
- [16] L. Garlappi, R. Uppal, and T. Wang. Portfolio selection with parameter and model uncertainty: A multi-prior approach. *The Review of Financial Studies*, 20(1):41–81, 2007.
- [17] L. P. Hansen and R. Jagannathan. Implications of security market data for models of dynamic economies. *Journal of political economy*, 99(2):225–262, 1991.
- [18] S. Hochreiter and J. Schmidhuber. Long short-term memory. *Neural computation*, 9(8):1735–1780, 1997.
- [19] A. J. Jacquier and M. Oumgari. Deep ppdes for rough local stochastic volatility. *Available at SSRN 3400035*, 2019.
- [20] P. Kidger, P. Bonnier, I. P. Arribas, C. Salvi, and T. Lyons. Deep signature transforms. In *Advances in Neural Information Processing Systems*, pages 3105–3115, 2019.
- [21] F. J. Király and H. Oberhauser. Kernels for sequentially ordered data. *Journal of Machine Learning Research*, 2019.
- [22] D. Levin, T. Lyons, and H. Ni. Learning from the past, predicting the statistics for the future, learning an evolving system. *arXiv preprint arXiv:1309.0260*, 2013.
- [23] S. Liao, T. Lyons, W. Yang, and H. Ni. Learning stochastic differential equations using rnn with log signature features. *arXiv preprint arXiv:1908.08286*, 2019.
- [24] M. Luo and J. Ma. On the dynamic frontiers of the limit order books-a principal agent problem view. *University of Southern California dissertations and theses, preprint*, 2021.

- [25] T. Lyons. Differential equations driven by rough signals (i): An extension of an inequality of lc young. *Mathematical Research Letters*, 1(4):451–464, 1994.
- [26] D. B. Madan and A. S. Cherny. Illiquid markets as a counterparty: An introduction to conic finance. *Robert H. Smith School Research Paper No. RHS*, pages 06–115, 2010.
- [27] R. C. Merton. Theory of rational option pricing. *The Bell Journal of economics and management science*, pages 141–183, 1973.
- [28] M. Min and T. Ichiba. Convolutional signature for sequential data. *arXiv preprint arXiv:2009.06719*, 2020.
- [29] M. Musiela and M. Rutkowski. *Martingale methods in financial modelling*. Springer, 2005.
- [30] E. Pardoux and S. Peng. Backward stochastic differential equations and quasilinear parabolic partial differential equations. In *Stochastic partial differential equations and their applications*, pages 200–217. Springer, 1992.
- [31] S. Peng. Filtration consistent nonlinear expectations and evaluations of contingent claims. *Acta Mathematicae Applicatae Sinica, English Series*, 20(2):191–214, 2004.
- [32] S. Peng and F. Wang. Bsde, path-dependent pde and nonlinear feynman-kac formula. *Science China Mathematics*, 59(1):19–36, 2016.
- [33] T. Pham and J. Zhang. Two person zero-sum game in weak formulation and path dependent Bellman-Isaacs equation. *SIAM J. Control Optim.*, 52(4):2090–2121, 2014.
- [34] J. Reizenstein and B. Graham. Algorithm 1004: The iisignature library: Efficient calculation of iterated-integral signatures and log signatures. *ACM Transactions on Mathematical Software (TOMS)*, 2020.
- [35] J. Ruan. Numerical methods for high-dimensional path-dependent pdes driven by stochastic volterra integral equations. *University of Southern California dissertations and theses, Volume12/etd-RuanJie-8638*, 2020.
- [36] M. Sabate-Vidales, D. Šiška, and L. Szpruch. Solving path dependent pdes with lstm networks and path signatures. *arXiv preprint arXiv:2011.10630*, 2020.

- [37] Y. F. Saporito and Z. Zhang. PDGM: a neural network approach to solve path-dependent partial differential equations. *arXiv preprint arXiv:2003.02035*, 2020.
- [38] E. Weinan, J. Han, and A. Jentzen. Deep learning-based numerical methods for high-dimensional parabolic partial differential equations and backward stochastic differential equations. *Communications in Mathematics and Statistics*, 5(4):349–380, 2017.
- [39] Y. Yu, B. Hientzsch, and N. Ganesan. Backward deep bsde methods and applications to nonlinear problems. *arXiv:2006.07635*, 2020.
- [40] J. Zhang. *Backward stochastic differential equations*. Springer, 2017.